Journal of Drug Delivery Science and Technology 114 (2025) 107617

Contents lists available at ScienceDirect

Journal of Drug Delivery Science and Technology

journal homepage: www.elsevier.com/locate/jddst

Intranasal delivery of dimethyl fumarate and monomethyl fumarate using hyaluronic acid-based hybrid nanoparticles to enhance CNS bioavailability

Carla Serri [a], Massimo Cossu [a], Vincenzo Guarino [b], Iriczalli Cruz-Maya [b], Giada Botti [c], Luca Ferraro [d], Paolo Giunchedi [a], Giovanna Rassu [a,*], Elisabetta Gavini [a], Alessandro Dalpiaz [c]

[a] Department of Medicine, Surgery and Pharmacy, University of Sassari, via Muroni 23/A, 07100, Sassari, Italy
[b] Institute of Polymers, Composites and Biomaterials, National Research Council, V.le J.F. Kennedy 54, 80125, Naples, Italy
[c] Department of Chemical, Pharmaceutical and Agricultural Sciences, University of Ferrara, Via L. Borsari 46, I-44121, Ferrara, Italy
[d] Department of Life Sciences and Biotechnology, and LTTA Center, University of Ferrara, Via Borsari 46, I-44121, Ferrara, Italy

ARTICLE INFO

Keywords:
Hybrid nanoparticles
Dimethyl fumarate
Monomethyl fumarate
Nose-to-brain delivery
Hyaluronic acid
Intranasal route

ABSTRACT

Dimethyl fumarate (DMF) and its active metabolite monomethyl fumarate (MMF) are first-line oral therapies for multiple sclerosis (MS), but their clinical use is limited by gastrointestinal side effects and low bioavailability. To overcome these limitations, this study reports the development and optimization of hyaluronic acid (HA)-modified lipid–polymer hybrid nanoparticles (LPNs) for intranasal administration, aimed at enhancing central nervous system (CNS) delivery of DMF via the nose-to-brain route. LPNs were prepared and fully characterized for physicochemical properties, including particle size (209–230 nm) and zeta potential (ranging from +0.28 to −19.6 mV), influenced by HA surface modification. The presence of HA in the LPNs enhanced DMF chemical stability, mucoadhesiveness, and significantly improved in vitro DMF release and permeation compared to free DMF suspension. Stability assays revealed rapid hydrolysis of DMF in rat whole blood, while MMF exhibited greater stability. Pharmacokinetic analysis in rats showed that following intravenous administration of free DMF, DMF was undetectable in blood and cerebrospinal fluid (CSF), with only MMF present in blood. Similarly, intranasal administration of free DMF suspension resulted in no detectable levels of DMF or MMF in blood and in the CSF. In contrast, intranasal delivery of LPNs enabled DMF brain targeting via the nose-to-brain pathway, with no systemic exposure. These findings demonstrate that HA-modified LPNs are a promising platform for the intranasal delivery of DMF, potentially reducing side effects and offering new therapeutic perspectives for the use of this drug in MS management.

1. Introduction

Multiple sclerosis (MS) is a chronic autoimmune disorder characterized by inflammation, demyelination, gliosis, and the loss of neurons, all of which significantly impact the Central Nervous System (CNS) [1]. The disease primarily targets myelinated axons within the CNS, leading to varying degrees of damage to both the myelin sheath and the axons themselves; neuronal bodies are also affected, particularly in advanced (progressive) stages of the disease [2]. MS usually occurs in young adults, with a mean onset age between 20 and 30 years. It can result in physical disabilities, cognitive decline, and a reduced quality of life [3]. MS is commonly categorized into four phenotypes: relapsing-remitting MS (RRMS), primary progressive MS, secondary progressive MS (SPMS), and progressive-relapsing MS [4]. Nine classes of disease-modifying therapies (DMTs) for MS (RRMS), are characterized by different mechanisms of action and routes of administration [3]. Among oral therapies, dimethyl fumarate (DMF, Tecfidera®) and its active metabolite monomethyl fumarate, (MMF, Bafiertam™) were approved by the U.S. Food and Drug Administration (FDA) on March 27, 2013 and on April 30, 2020, as a treatment RRMS and SPMS, respectively [5,6]. In vitro studies demonstrated that DMF primarily impacts the properties of immune modulatory cells and the differentiation of lymphocytes and microglial cells [3,5]. MMF, the sole active metabolite of DMF, has been known to interact with various immunomodulatory

This article is part of a special issue entitled: Skin and mucosal drug delivery published in Journal of Drug Delivery Science and Technology.

* Corresponding author.
E-mail addresses: cserri@uniss.it (C. Serri), mcossu@uniss.it (M. Cossu), vincenzo.guarino@cnr.it (V. Guarino), cdiriczalli@gmail.com (I. Cruz-Maya), bttgdi@unife.it (G. Botti), frl@unife.it (L. Ferraro), pgiunc@uniss.it (P. Giunchedi), grassu@uniss.it (G. Rassu), eligav@uniss.it (E. Gavini), dla@unife.it (A. Dalpiaz).

https://doi.org/10.1016/j.jddst.2025.107617
Received 7 August 2025; Received in revised form 22 September 2025; Accepted 4 October 2025
Available online 5 October 2025

nuclear transcription factor pathways [6,7]. After oral administration, DMF is rapidly absorbed and converted by esterases in the small intestine into MMF [5,8], that reaches peak concentration within 5–6 h; the half-lives of DMF and MMF are 12 min and 36 h, respectively [9]. DMF is associated with side effects primarily related to the gastrointestinal tract, including diarrhoea, nausea, abdominal pain, and vomiting. Some 43 % of patients, who also experienced flushing and leukopenia, discontinued treatment within the first three months [10,11]. Furthermore, DMF has limited water solubility and low stability, resulting from its tendency to undergo hydrolysis and sublimation at room temperature [12]. To overcome the problems of poor physicochemical stability [13] and bioavailability of DMF, Ojha and collaborators have highlighted the advantages of encapsulating DMF in nanoparticles (NPs) [14] and solid lipid nanoparticles (SLNs) [15]. They observed an enhancement in the activity of DMF, and in relative bioavailability when DMF-SLNs were orally administered to Wistar rats [15]. Furthermore, in our previous research, the chemical and physical stability of DMF was enhanced by encapsulating DMF in lipid–polymer hybrid nanoparticles (LPNs) containing hyaluronic acid (HA). In addition, preliminary in vivo experiments in rats indicated that the HA-based hybrid nanoparticles could enhance the brain bioavailability of DMF following intranasal administration [16]. Nasal drug delivery is a safe and non-invasive method for administering therapeutic doses, making it particularly advantageous for treating neurological and chronic diseases [13,17]. Intranasal administration offers a beneficial approach for drug delivery by improving side effect profiles, particularly by minimizing gastrointestinal issues, and ensuring a rapid onset of action in the brain [13]. In fact, through direct nose-to-brain transport, rapid drug delivery to the brain and onset of drug effects are achieved, maintaining therapeutic drug concentrations in the brain while minimizing the required clinical doses; this concurrently reduces systemic exposure and peripheral adverse effects associated with the drug [18].

In this study, HA-based LPNs were optimized to facilitate the intranasal delivery of DMF and to quantify the MMF generated from the degradation of encapsulated DMF, owing to its pharmacological activity. The role of the lipid and polymer components in stabilizing DMF was emphasized, and the concentrations of both active components, DMF and MMF, were investigated in simulated biological fluids during in vitro release and permeation studies. Subsequently, the in vitro stability of DMF and MMF in rat whole blood was evaluated prior to conducting in vivo pharmacokinetic studies after intravenous administration. Additional in vivo pharmacokinetic studies in rats were then performed following nasal administration of DMF, either as the pure drug or encapsulated in LPNs, to provide evidence of DMF behaviour in vivo and its potential for nose-to-brain transport.

2. Materials and methods

2.1. Materials

Dimethyl fumarate (purity 97 %) (DMF), monomethyl fumarate (MMF), poloxamer F407 (P) (Poly (ethylene glycol)-block-poly (propylene glycol)-block poly (ethylene glycol)), mucin (from pig stomach, type II), acetonitrile, ethanol, methanol, basic sodium phosphate (Na_2HPO_4), sodium chloride (NaCl), and potassium chloride (KCl) were purchased by Sigma-Aldrich (Merck Life Science srl, Milan, Italy). Sodium Alginate (Protanal LF 120 LS, MW: 221 kDa; viscosity (1 % sol)) was obtained by FMC BioPolymer (Philadelphia, USA). Phosphatidylcholine (Lipoid S S100®) was gifted by Lipoid GmbH (Ludwigshafen, Germany) (CP); Cholesterol (Chol) was obtained by WVR (Milan, Italy). Hyaluronic acid sodium salt (HA) with a molecular weight of 1500–1800 kDa was bought from BioChemical Fluka (Milan, Italy). Pure water was obtained using a MilliQ R4 purification system (Millipore, Milan, Italy). Dulbecco's Phosphate-Buffered Saline (DPBS) was obtained from ThermoFisher Scientific (Milan, Italy). Merck Life Sciences Srl supplied bovine serum albumin (BSA), dimethyl sulfoxide (DMSO), trifluoroacetic acid (TFA), and ferulic acid (Fer). DMF and MMF stock solutions in DMSO (0.01 M final concentration) were stored at −20 °C until their use for in vivo or in vitro studies.

2.2. Formulation development

2.2.1. Interaction measurements

Differential scanning calorimetry (DSC) was employed to investigate main interactions through the different materials used. Accordingly, DSC analyses were carried out on powders of phosphatidylcholine (CP), cholesterol (Chol), poloxamer (P), hyaluronic acid (HA), and their dried complexes including CP/Chol, CP/Chol/P, CP/Chol/P/HA. The CP/Chol and CP/Chol/P complexes were prepared by dissolving the respective materials in 5 mL of ethanol at 50 °C, while the CP/Chol/P/HA complex was prepared by first solubilizing CP/Chol and P in ethanol, followed by the addition of this solution to an aqueous phase, containing HA and P. All complexes were subsequently dried and lyophilized (5PASCAL equipped with LIO5P DIGITAL, Bologna, IT) at 7.6 Torr (0.01 Atm) for 24 h. A Discovery DSC calorimeter (TA Instruments, Delaware, USA) calibrated with an indium standard was used in this study. The calorimeter cell was flushed with nitrogen at a flow rate of 100 mL/min. The temperature ramp was performed from −20 °C to 300 °C at a heating rate of 10 °C/min.

2.2.2. Preparation of LPNs

The modified nanoprecipitation technique was used to prepare unloaded and DMF-loaded LPNs [19]. The compositions and the corresponding acronyms are reported in Table 1; the L_A series consist of solely CP as lipid, while the L series comprise combinations of CP, Chol, and P; the letter H denotes the presence of HA whereas D indicated the DMF-loaded LPNs. Briefly, the exact amounts of CP alone or CP, Chol, and P were dissolved in 5 mL of ethanol; LD and LHD (and the corresponding LD_A and LDH_A) were prepared dissolving also DMF in the organic phase. Then, the organic phase was added to the aqueous phase (10 mL), which consisted of a poloxamer water solution with and without HA; then the mix was vortexed for 10 min (TechnoKartell Milan, Italy). The resulting suspension was sonicated at 50 % ultrasound for 2 min at 4 °C using a probe sonicator (Bioblock Vibracell, Fisher Bioblock Scientific, Illkirch, France) and stirred 5 h for complete ethanol evaporation. Finally, LPNs dispersion was extruded once through the regenerated cellulose syringe filter (pore size: 0.45 μm; filter size: 25 mm; AlfaTech, Genova, Italy) and stored at 4 °C. The reproducibility of the preparation method was tested by conducting the formulation process three times. All formulations were not isolated but used as dispersions in all experiments.

2.3. Characterization of LPNs: size, ζ potential, and morphology

The mean diameter and size distribution of LPNs were determined by photon correlation spectroscopy (PCS) using a Coulter N5 (Beckman Coulter, Miami, USA). All samples were diluted in filtered Milli-Q water

Table 1
The compositions and acronyms of the formulations.

Acronym	Organic Phase (O)				Water Phase (W)	
	CP (mg)	Chol (mg)	P (mg)	DMF (mg)	HA (mg)	P (mg)
L_A	400	–	–	–	–	1.5
LD_A	400	–	–	40	–	1.5
LH_A	400	–	–	–	30	1.5
LHD_A	400	–	–	40	30	1.5
L	400	150	150	–	–	1.5
LD	400	150	150	40	–	1.5
LH	400	150	150	–	30	1.5
LHD	400	150	150	40	30	1.5

CP: phosphatidylcholine; Chol: cholesterol; P: poloxamer; DMF: dimethyl fumarate; HA: hyaluronic acid sodium salt (HA).

(0.22 μm pore size, polycarbonate filters, MF-Millipore, Microglass Heim, Italy) and analysed with the detector at 90°. The polydispersity index (PDI) was used to evaluate the particle size distribution. ζ potential (ζp) was measured with a Zetasizer Nano ZS (Malvern Instruments, Malvern, UK) on a 0.1 mg/mL LPNs suspended in Milli-Q water at room temperature. The results were expressed as mean ± standard deviation (SD) of three measures (n = 3).

The morphology of all LPNs was analysed using Transmission Electron Microscopy (TEM, FEI Tecnai G12 Spirit Twin, Eindhoven, the Netherlands), which is equipped with a LaB6 source and a FEI Eagle 4k CCD camera. The acceleration voltage was set to 120 kV. For the sample preparation, 100 μL of each ultra-diluted sample (LH, LHD, LP, and LPD) was dropwise collected onto a copper TEM grid (300 mesh, 3 mm diameter) until the liquid is not completely evaporated.

2.4. Assessing total drug in dispersion

The total amount of DMF and MMF in the LPNs was quantitatively assessed in all LD, LHD, LD_A and LHD_A. The method employed to determine the total drug amount was based on the method outlined in Serri et al. [16]. Briefly, 100 μL of LPNs was blended with 9.90 mL of acetonitrile, shaken at room temperature for 30 min and sonicated for 2 min at 35 Hz to completely dissolve the LPNs. The solution was directly injected in HPLC. The quantification of DMF and MMF was performed following the method developed by Habib and collaborators [20] and using a HPLC–DAD system (Varian, Palo Alto, CA, USA), featuring two ProStar 210 pumps, a ProStar 410 autosampler, and a Varian 330 detector. Separation occurred on a Thermo Fisher Scientific Hypersil C18 column (150 mm × 4.6 mm, 5 μm), with a guard column (2 cm × 4.0 mm, 5 μm). The mobile phase, consisting of water (filtered through a 0.22 μm nylon filter) adjusted to pH 2.6 with phosphoric acid and methanol (50:50, v/v), was run isocratically at 1.5 mL/min at ambient temperature. The injection volume was 10 μL and the analysis time was 4 min per sample. Peak areas in the chromatography were recorded and measured at 210 nm. Concentrations of DMF and MMF were calculated by standard curves interpolation in the range of 2.5–50 μg/mL (DMF: $y = 449786.6x - 309866.3$; $R^2 = 0.999$. MMF: $y = 212523.1x - 309942.3$; $R^2 = 0.999$).

The amount of DMF and MMF in the dispersion were expressed as μg/mL and as percentage respect to the amount of DMF used during LPNs preparation [21] (mean ± SD; n = 3).

2.5. Stability study

The physical stability of LPNs was studied by monitoring changes in their hydrodynamic diameter when stored at 4 °C for 30 days. The results are average values obtained from at least three independent measurements. Moreover, the chemical stability of the total drug in LD LHD, and LD_A LHD_A were studied for 30 days at 4 °C. The total drug in the samples were analysed at each predetermined time point (0, 7, 14, 23, 30 days). The protocols like described in the paragraph 2.4.

2.6. In vitro DMF release assay

In vitro release of DMF from LHD, DMF suspension (2.5 mg/mL) and LH with added DMF (LH + DMF 2.5 mg/mL) was tested. Briefly, an aliquot of LHD, LH + DMF and DMF suspension (containing 10 mg of DMF) were placed in the dialysis membrane tube (Float-A-Lyzer® G2 Dialysis Device MWCO 50 kD, Spectrum Laboratories, Rancho Dominguez, CA, USA), which was then transferred to a clear vial containing 40 mL of phosphate-buffered saline (PBS) pH 7.4. Samples were incubated in a stirring incubator (Argo Lab, SKI 4, VWR, Milan, Italy) at 37 °C ± 0.5 °C with shaking at 100 rpm for 72 h. At predetermined time points (0–72 h), 1 mL of the release medium was sampled and replaced with an equivalent volume of fresh dissolution medium. The concentration of DMF and MMF in the release medium was determined by HPLC method, already described in Section 2.4. Then the cumulative amount of DMF and MMF over time was calculated. The results were obtained in triplicate and were expressed as mean ± SD.

2.7. Viscosity and mucoadhesion properties

The viscosity performance of L, LH, LD and LHD were evaluated using a rotational viscometer (Alpha-L, Fungilab, Barcelona, Spain) with spindles L1 and L2. The measurements were conducted at a constant rotational speed of 100 rpm and a temperature of 37 °C, utilizing a sample volume of 30 mL of the LPNs. The results are presented as the mean ± SD of three measurements (n = 3). The mucoadhesion of the LPNs was assessed measuring the detachment force using a precision balance modified [16]. Briefly, a regenerated cellulose membrane (porosity 0.45 μm; diameter = 1.5 cm; Whatman™, Dassel, Germany) was saturated with artificial nasal mucus and fixed to the balance plate. A volume of 100 μL of LPNs was applied to the surface of the probe (diameter = 1.5 cm) with double-sided adhesive tape, put in contact with the membrane (contact force of 10 g for 120 s), and then the detachment force was recorded [16]. Additionally, a sodium alginate solution (100 μL, 3 mg/mL, with a viscosity of 9.6 ± 0.4 cP) and HA solution (100 μL, 3 mg/mL) were tested as a positive control, whereas 100 μL of MilliQ water (blank) as negative control. Results of mucoadhesion were expressed as stress (Pa), represented as mean ± SD from five replicates (n = 5).

2.8. Assessment of in vitro permeation of DMF

The in vitro permeation experiments for LHD and DMF suspension (2.5 mg/mL) were conducted using permeation test cells (prototypes developed and patented by the University of Sassari, under patent number EP3909667A1). In brief, 1 mL of LHD and LD (containing 2.5 mg of DMF) was placed on either a synthetic hydrophobic or hydrophilic membrane (Polyvinylidene difluoride membrane filter discs, PVDF 0.45 μm, from Merck Millipore, Burlington, USA), chosen to simulate the different components of the nasal mucosa, like mucus (hydrophilic layer), cell membranes and neurons (lipophilic structures), which the LPNs would cross after the administration [22]. The membrane separated the donor compartment from the acceptor compartment, contained 40 mL of PBS, maintained at a temperature of 37 °C. For comparison, the test was also performed using DMF (2.5 mg) suspended in water. At predetermined time points (0–180 min), 1 mL of the acceptor medium was taken and the amount of DMF permeated was quantified using the HPLC method, reported in Section 2.4. The concentration of MMF present in medium was also measured. The acceptor medium was replaced with an equivalent volume of fresh medium. The experiment was conducted in triplicate.

2.9. Degradation studies in rat whole blood

2.9.1. DMF degradation in rat blood (4 °C)

Heparinized rat whole blood (100 ⌈L amounts) obtained from male Sprague-Dawley rats (200–250 g body-weight) was spiked at 4 °C with DMF stock solution to obtain DMF final concentrations in the 10–100 μM (1.44–14.41 μg/mL) range and incubated just the time necessary to vortex each sample that was. The samples (100 μL) were then immediately mixed with ice-cold acetonitrile (250 μL), followed by the addition of the internal standard (50 μL of 100 μM Fer dissolved in a mixture of water and acetonitrile in 25:75 v/v ratio). The samples were subsequently centrifuged twice at 16,000×*g* for 5 min at room temperature, transferring approximately 300 μL of supernatant between the centrifugations. As a control, a blood sample (100 μL) was immediately added with 300 μL of ice-cold acetonitrile and then centrifuged as described above. DMF and its potential hydrolysis product (MMF) were quantified by injecting 10 μL of treated or control samples into the HPLC system (see Section 2.10.3). The MMF amounts produced by the DMF hydrolysis

were expressed as MMF/DMF molar percentage ratios, where the DMF molar amounts were calculated considering the dilution factors of the stock solutions added to the blood samples.

2.9.2. MMF degradation in rat blood (37 °C)

Three milliliters of heparinized rat whole blood obtained from adult male Sprague-Dawley rats (200–250 g body weight) maintained at 37 °C, were spiked with MMF stock solution to achieve a final MMF concentration of 30 μM (3.90 μg/mL). Samples were then withdrawn at predefined time points (up to 120 min of incubation) and immediately processed as described in Section 2.9.1. MMF was quantified by injecting 10 μL of treated or control samples into the HPLC system (see Section 2.10.3).

2.10. In vivo experiments

2.10.1. Intravenous administration of MMF and DMF

In a first set of in vivo experiments, DMF or MMF was intravenously administered to different groups (n = 4/group) of adult male Sprague-Dawley rats (200 g body weight) anesthetized with 1.5 % mixture of isoflurane and air. DMF or MMF 4 mg/ml solutions were prepared by first dissolving DMF or MMF in EtOH and then adding saline solution (0.9 % NaCl) to a final 50:50 (v/v) ratio. DMF or MMF were then intravenously administered at the doses of 2 mg/kg (i.e. 2.8 μmol/rat) or 1.8 mg/kg (i.e. 2.8 μmol/rat), respectively, by infusing the DMF or MMF solution into the rat femoral vein over 5 min at rates of 20 μL/min or 18 μL/min, respectively. At the end of the administrations and at predetermined time points, blood samples (100 μL), along with cerebrospinal fluid (CSF) samples (30 μL), were collected. The cysternal puncture method described by van den Berg et al. [23] was used for the CSF withdrawn. This method requires a single needle stick allowing the collection of serials (30–40 μL) CSF samples that are virtually blood-free] [24]. A total volume of about a maximum of 150 μL of CSF/rat (*i.e.*, four 30/40 μL samples/rat) was collected during the experimental session, choosing the time points (n = 3–7, taking into account a maximum of four collections for rat) in order to allow the restoring of the CSF physiological volume. The compounds were quantified by injecting a volume of 10 μL of blood samples treated as described above (section 2.9.1), and untreated CSF samples in the HPLC apparatus (see Section 2.10.3).

2.10.2. Nasal administration of DMF

DMF was nasally administered as free compound or LHD formulation to different groups (n = 4/group) of adult male Sprague-Dawley rats (200 g/body weight). To this purpose, anesthetized rats were laid on their backs and received in each nostril 50 μL of a water suspension of free DMF (2 mg/mL; *i.e.* approximately 0.2 mg/rat) or LHD formulation (DMF content about 2 mg/mL). The nasal administration was performed using a semiautomatic pipette connected to a short polyethylene tubing, which was inserted approximately 0.6–0.7 cm into each nostril. At the end of the administration and at predetermined time points, blood samples (100 μL), along with CSF samples (30 μL), were collected; compounds quantification was performed by injecting 10 μL of blood samples treated as described above (Section 2.9.1) and untreated CSF samples in the HPLC apparatus (see Section 2.10.3). The Italian Ministry of Health approved the experimental procedures, (n° 287/2024-PR; March 25, 2024) conducted according to the European Communities Council Directive (2010/63/EU). These procedures aimed to minimize animal pain, discomfort, and the number of subjects, following ARRIVE guidelines.

2.10.3. MMF and DMF quantification by HPLC analysis

MMF and DMF concentrations in rat blood and CSF samples were quantified using an HPLC method. Specifically, the modular chromatographic system, paired with an injection valve containing a 20 μL sample loop (model 7725; Rheodyne, IDEX, Torrance, CA, USA), consisted of a pump (model LC-40D, Shimadzu, Kyoto, Japan) and a diode-array detector (DAD, model SPD-M40, Shimadzu, Kyoto, Japan). LabSolutions Software (version 5.110, Windows 10, Shimadzu, Kyoto, Japan) was utilized for data acquisition and processing. Sample separations were performed at room temperature on a 5 μm Hypersil BDS C18 column (150 mm × 4.6 mm i.d.; ThermoFisher Scientific Srl, Milan, Italy), which was protected by a guard column filled with the same stationary phase. The mobile phase consisted of a water/acetonitrile (acidified with 0.1 % v/v TFA) mixture [80:20 (v/v) ratio] and was eluted under isocratic conditions at a flow rate of 0.8 mL/min. Chromatograms were recorded at 216 nm for the quantification of MMF and DMF, and at 320 nm for Fer, which served as an internal standard in the extraction procedures of rat whole blood samples. The retention times for MMF, Fer, and DMF under these analytical conditions were 3.8, 6.4, and 8.2 min, respectively.

Repeated analysis (n = 6) of the same sample solution containing MMF or DMF at a concentration of 50 μM (6.66 μg/mL for MMF and 7.21 μg/mL for DMF), singularly dissolved in a mixture of water and acetonitrile (25:75 v/v), was used to determine the chromatographic precision, which was represented by relative standard deviation (RSD) values ranging from 0.90 to 0.95 for all the tested compounds.

A preliminary analysis of blank rat blood and CSF samples confirmed the absence of interferences at the retention times of MMF, DMF, and the internal standard (Fer).

A CSF simulation fluid, composed of standard aliquots of the balanced Dulbecco's Phosphate-Buffered Saline (DPBS) solution depleted of calcium and magnesium and supplemented with 0.45 mg/mL bovine serum albumin (BSA), was used for calibration purposes [25,26]. The calibration curves of peak areas as a function of analytes concentrations in simulated CSF were established for MMF and DMF in the concentration range of 0.3–150 μM (0.04–19.97 μg/mL for MMF and 0.04–21.62 μg/mL for DMF) and were found to be linear (n = 6, r = 0.999, $p < 0.0001$).

MMF recovery experiments in rat whole blood samples were conducted by comparing the peak areas obtained from blood test samples (50 μM, corresponding to 6.66 μg/mL, n = 4) to those obtained by injecting an equivalent concentration of MMF dissolved in a water/acetonitrile (25:75 v/v) mixture. The results revealed an average MMF recovery of approximately 83 %. Based on this result, MMF blood concentration was calculated using the peak area ratio relative to the internal standard (Fer). The MMF calibration curve was generated by adding MMF to rat whole blood (4 °C) at eight different concentrations ranging from 1 to 500 μM (0.13–66.55 μg/mL), resulting in a linear relationship (n = 8, r = 0.998, $p < 0.0001$).

2.10.4. In vivo pharmacokinetic calculations

Nonlinear regression (exponential decay) of concentration values, quantified at appropriate time intervals after infusion, was used to determine the in vivo half-life ($t_{1/2}$) of MMF in the rat bloodstream, further validated by applying linear regression to the semi-logarithmic plot. The area under the concentration-time curves (AUC, $\mu g \bullet mL^{-1}$ min) in rat bloodstream or CSF, following MMF and DMF intravenous administrations or DMF nasal administrations as free compound or LHD formulation, was calculated using the trapezoidal method. GraphPad Prism version 10.0 (GraphPad Software, San Diego, California, U.S.A.) was utilized to perform all the calculations.

2.11. Data analysis and statistics

The results are presented as mean ± SD or as representative values. All data were measured in triplicate and viscosity and mucoadhesion in five repetitions of an experiment. The statistical data analysis was performed using GraphPad Prism 10.4.1 software (GraphPad Software, Inc., San Diego, CA, USA). An unpaired *t*-test was performed for the statistical difference between the two treatment groups. Tukey's multiple comparison tests followed a one and two-way ANOVA analysis of variance

test in case of multiple comparisons. Statistical significance was set at $p < 0.05$.

3. Results and discussion

3.1. Assessing interactions and characterization of LPNs

The characterization of the LPNs began with thermal analyses to evaluate possible interactions between the lipid and polymer components (Fig. 1). In the DSC thermograms, endothermic peaks were associated with the presence of semicrystalline phases that require the input of heat to change their physical state. In the case of CP/Chol complex, formed by the assembly of apolar phases like CP and Chol, no remarkable peaks were detected. In contrast, when CP/Chol was combined with the P complex containing positively charged polar groups, a broad peak can be recognised with a maximum peak at 96.4 °C. In the case of CP/Chol/P/HA complex including HA with negative polar groups, a more pronounced peak appeared, with a maximum at 106.7 °C.

Accordingly, an increase of heat of fusion or enthalpy, calculated as area of the characteristic peaks, was recorded (Table 2). Hence, the combination of P with HA suggests the formation of more stable crystalline phases due to their polar interactions, and in agreement with characteristic peaks of the single components (Fig. S1).

Based on these data, LPNs were prepared and characterized. Particle size, PDI and ζp were determined and are reported in Table 3. LPNs without Chol and P showed smaller sizes, ranging from 106 nm in L_A to 111 nm in LD_A. In contrast, incorporation of Chol and P into the formulations increased the of Chol and P into the LPNs reduced the PDI (Table 3), lowering it from values above 0.600 (L_A, LD_A, LH_A and LHD_A) to approximately 0.300 (L, LD, LHD). Conversely, the addition of HA (LH) increased PDI [27]. However, when DMF and HA were present (LHD), a significant reduction in PDI was observed, likely due to interactions between HA and DMF [16]. Furthermore, ζp was influenced by HA addition, becoming more negative (from −2.60 mV in L to −25.0 mV in LH), and also by DMF loading (from 0.28 mV in LD to −19.6 mV in LHD). Higher absolute ζp values enhance the stability of dispersed nanoparticles by preventing aggregation and promoting uniform dispersion [28,29].

Fig. 2 shows representative TEM images of LH, LHD, L, and LD. The images at two different magnifications revealed discrete, spherical shape for L (Fig. 2a). The presence of HA in LH promoted the formation of a core-shell structure with HA forming the outer shell (Fig. 2c). Meanwhile, the presence of DMF, preferentially distributed onto the particle surface, significantly contributes to form more irregular shape of particles (Fig. 2b–d). The TEM images, together with the ζp values, provide evidence supporting the presence of the outer HA layer, consistent with the literature [16,19,30].

Table 2
Heat of fusion of semi-crystalline phases in the different formulations.

Sample	Enthalpy of fusion (J/g)
CP/Chol	4.51
L	29.20
LH	85.57

Table 3
Characterization of LPNs. Results are expressed by mean ± SD.

Formulation	Size (nm)	PDI	ζp (mV)
L_A	111.0 ± 0.3	0.70 ± 0.03	−0.68 ± 0.82[a]
LD_A	106.0 ± 0.7[d]	0.71 ± 0.07	+2.38 ± 0.30[d]
LH_A	148.4 ± 1.0[e]	0.52 ± 0.02	−5.38 ± 1.17[e]
LHD_A	130.8 ± 2.3[f,g]	0.98 ± 0.01[f,g]	−6.97 ± 0.37[f,g]
L	246.0 ± 9.7[b]	0.36 ± 0.02	−2.60 ± 0.20
LD	209.3 ± 2.7[c]	0.37 ± 0.01	+0.28 ± 0.10[c]
LH	245.9 ± 7.4[h,i]	0.52 ± 0.03[i]	−25.0 ± 1.60[h,i]
LHD	230.0 ± 4.0[j,k,l]	0.38 ± 0.05[j]	−19.60 ± 0.50[j,k,l]

[a] $p < 0{,}0001$ L_A vs LD_A.
[b] $p < 0.0001$ L_A vs L.
[c] $p < 0.0001$ L vs LD.
[d] $p < 0.0001$ LD vs LD_A.
[e] $p < 0.0001$ L_A vs LH_A.
[f] $p = 0.0004$ LH_A vs LHD_A.
[g] $p < 0.0001$ LD_A vs LHD_A.
[h] $p < 0.0001$ LH_A vs LH.
[i] $p < 0.0001$ L vs LH.
[j] $p < 0.0001$ LHD_A vs LHD.
[k] $p < 0.0001$ LH vs LHD.
[l] $p < 0.0001$ LD vs LHD.

No significant changes were recognised in size over the 30-day period for the L, LH, LD, and LHD formulations (Fig. 3a). In contrast, the L_A, LH_A, LD_A, and LHD_A (Fig. 3b) exhibited instability in size over time. According to the literature, Chol and P enhance the stability and rigidity of the carrier [19,31]. Notably, only the LH demonstrated a slight increase in diameter by day 30 ($p < 0.001$).

3.2. Total drug in dispersion, encapsulation efficiency and DMF stability over time

Table 4 reports the total amount of DMF and MMF in the LPNs, expressed both as μg/mL and as a percentage relative to the initial total amount of DMF weighed during preparation. LHD and LD showed significantly higher DMF concentrations than LHD_A and LD_A, corresponding to 61.7 % and 65.9 % of the initial total amount of DMF,

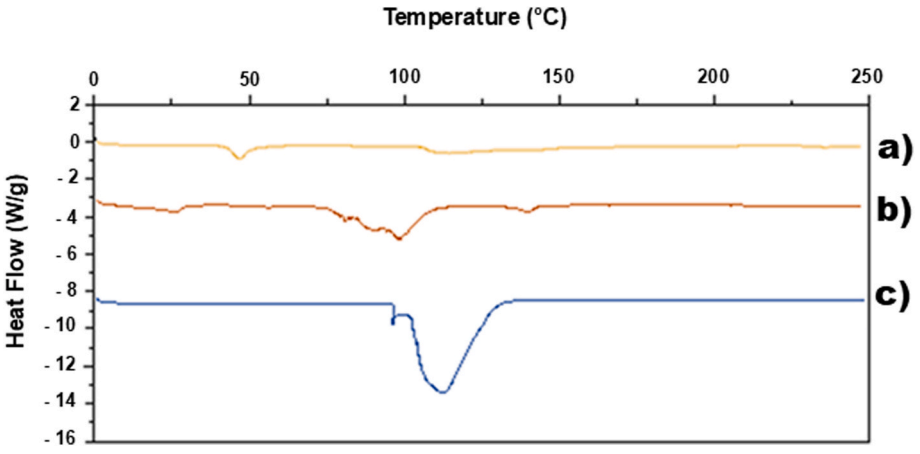

Fig. 1. DSC analyses to investigate polar interactions: Thermograms of **a)** CP/Chol, **b)** CP/Chol/P and **c)** CP/Chol/P/HA complexes.

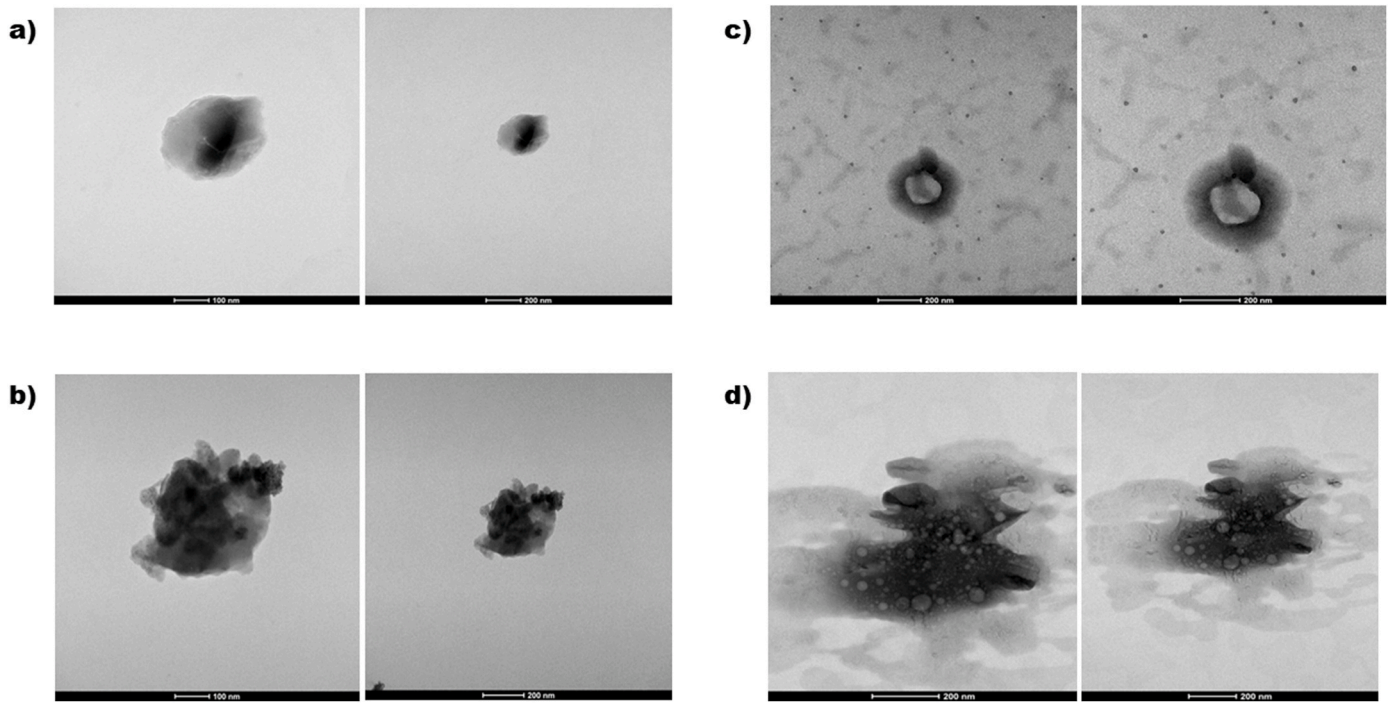

Fig. 2. Representative TEM images of **a)** L, **b**) LD, **c**) LH and **d**) LHD.

respectively. All LPNs contained a small amount of MMF, resulting from the degradation of approximately 3 % of the initial DMF.

The chemical stability of DMF was maintained for 30 days only in LHD (Fig. 3c): the total DMF content in LHD remained constant over 30 days, whereas in LD it decreased significantly, from 64.6 % to 19.5 % ($p < 0.001$). In LHD_A, DMF degradation occurred within 7 days, with the concentration dropping to only 0.5 %. These findings confirm that only a complete hybrid lipid-polymer structure can effectively trap DMF and protect it from hydrolysis [16]. Furthermore, the MMF content in LHD also remained stable, which is advantageous for in vivo applications given the established pharmacological activity of MMF [20].

3.3. In vitro drug release assay

The DMF release profiles from LHD, LH + DMF and DMF suspension are depicted in Fig. 4a, while the MMF concentrations in the medium over time are presented in Fig. 4b. The data indicate that LHD exhibited a burst release of DMF (38.65 ± 1.96 μg/mL, corresponding to 15.66 ± 0.79 % of the DMF content) within 10 min, which was markedly higher than that from the DMF suspension (11.86 ± 10.95 μg/mL) and LH + DMF (3.3 ± 0.56 μg/mL). In addition, LHD maintained a constant DMF release profile up to 1 h (50.66 ± 4.45 μg/mL, corresponding to 21.08 ± 1.84 % of DMF content), while the corresponding concentrations for DMF and LH + DMF were significantly lower (36.54 ± 1.15 μg/mL (18.67 ± 0.56 %) and 21.05 ± 1.96 μg/mL (10.74 ± 0.98 %), respectively). Thereafter, the DMF concentration gradually decreased to a value of 16.82 ± 2.74 μg/mL, 24 h after the start of the test (Fig. S2), and it was accompanied by an increase in MMF concentration (Fig. S2), probably due to the hydrolysis of DMF to MMF in PBS (pH 7.4) [32,33]. The amount of MMF in PBS during the LHD test progressively rose to 19.35 ± 1.04 μg/mL (Fig. 4b) and 42.28 ± 4.58 μg/mL at 2.5 and 24 h, respectively, followed by a decline to 27.08 ± 3.72 μg/mL at 72 h, respectively. The concentration of MMF was significantly lower in the case of LH + DMF and DMF suspension than in LHD (24.36 ± 4.64 and 21.91 ± 1.53 μg/mL at 72 h, respectively) (Fig. S2).

The relatively enhanced release of DMF from LHD compared to the DMF suspension can be attributed to the large specific surface area of the nanoparticles, which promotes the dissolution and release of DMF [34]. This effect is further accelerated by the presence of surfactants in the formulation, to the extent that it surpasses the dissolution rate of free DMF. However, considering the low percentage of DMF released during the observed time frame, this phenomenon primarily affected only the small fraction of DMF located near the nanoparticle surface.

3.4. Viscosity and mucoadhesion properties

Viscosity and mucoadhesive properties are crucial for enhancing the efficacy of intranasal drug delivery systems. Increased viscosity prolongs the formulation's residence time in the nasal cavity, while strong mucoadhesion ensures sustained contact with the mucosa, improving drug absorption [35,36]. The LH and LHD formulations exhibited optimal viscosity values of 117.53 ± 0.80 cP and 97.03 ± 0.12 cP, respectively, while the viscosities of the L and LD formulations were recorded at 27.73 ± 0.41 cP and 13.2 ± 0.78 cP, respectively. Furthermore, the viscosity of the LHD and LD decreased by about 15.13 cP following the incorporation of DMF. Therefore, the viscosity of LHD was found to be optimal for a nasal formulation, as increased viscosity is necessary to ensure prolonged residence time in the nasal cavity, without significantly compromising the formulation's spreadability [13, 16].

The mucoadhesion test (Fig. 3d) pointed out that all formulations exhibited mucoadhesive properties. LH and LHD showed detachment stresses of 1519.3 and 1446.9 Pa, respectively, values comparable to those of the HA solution alone.

HA enhances both viscosity and mucoadhesion, stabilizing nanoparticles and maintaining mucosal hydration, thereby enhancing the availability of encapsulated drugs [37]. Additionally, HA's ability to support mucosal barrier integrity complements the natural mucociliary clearance mechanism, facilitating effective drug retention and absorption [38]. Research indicates that P improves the structural integrity and mucoadhesion of nasal delivery systems, resulting in increased residence time and therapeutic efficacy [39,40]. The synergistic effect of HA and P in intranasal formulations maximizes drug delivery by maximising both viscosity and mucoadhesion, ultimately leading to improved

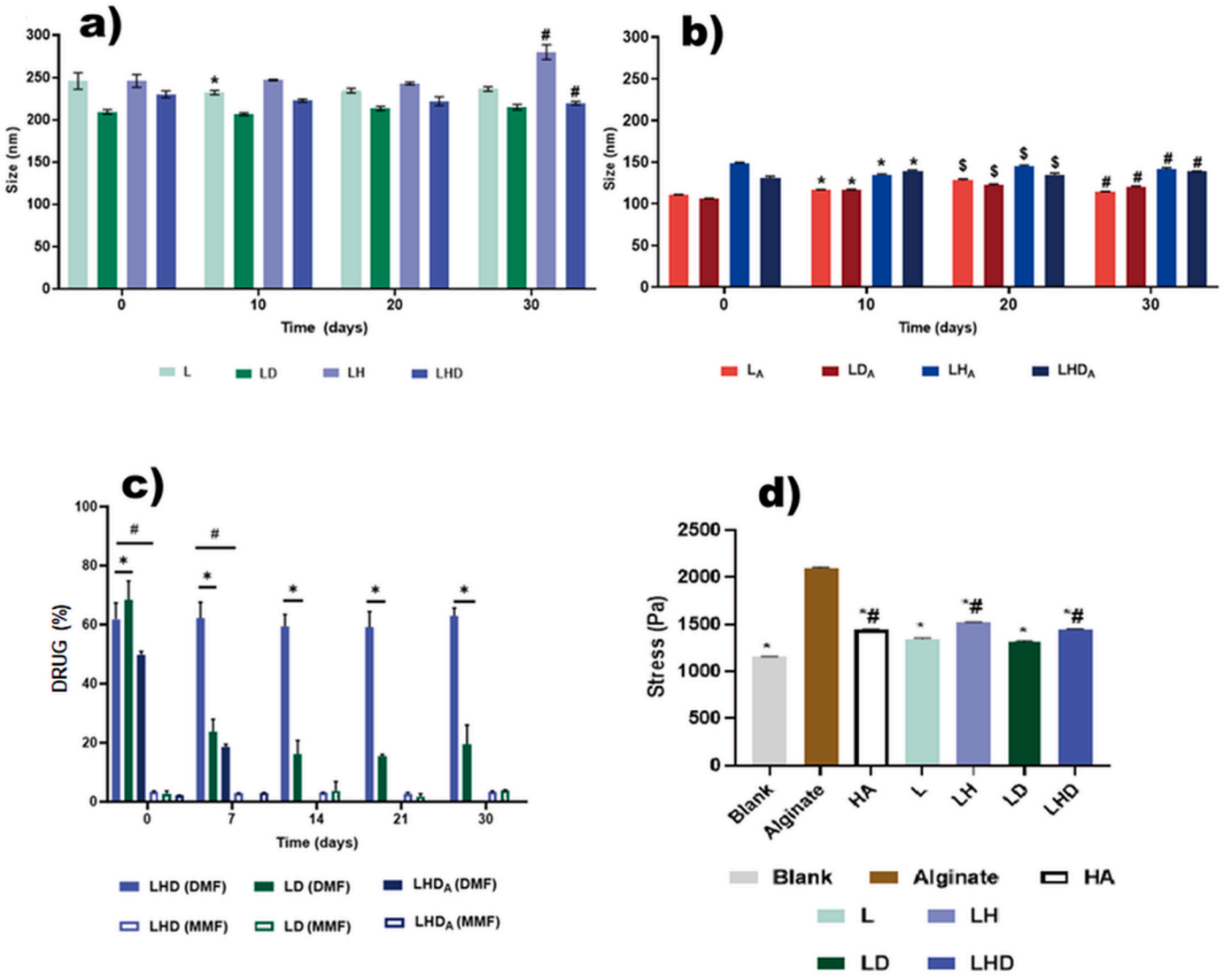

Fig. 3. a) The mean diameter of **a)** L, LH, LD, LHD and **b)** L_A, LD_A, LH_A, LHD_A, stored at 4 °C for 30 days *p < 0.001 day 0 vs 10, $p < 0.001 day 10 vs 20, #p < 0.001 day 20 vs 30; **c)** Amount of DMF and MMF (%) in LD, LHD and LHD_A measured over 30 days. *p < 0.001 LHD vs LD; #p < 0.001 LHD t0 vs LHDA 7 days and LD 14 days vs LD 21 days and LD 30 days; **d)** Stress (Pa) needed to detach LPNs, HA and alginate solutions from membrane saturated with artificial nasal mucus (n = 3). (*p < 0.0001 Alginate vs Blank/L/LH/LD/LHD; #p < 0.0001 Blank vs LH/LHD/HA; §p < 0.0001 LH vs LHD; $ p < 0.0001 HA vs Blank/Alginate/LH/LHD). The results are reported as mean ± SD.

Table 4
Total drug of DMF and MMF in LDA, LHD_A, LD and LHD dispersion (mean ± SD, n = 9).

	DMF µg/mL	DMF (%)	MMF µg/mL	MMF (%)
LD_A	1623.2 ± 1.5[a,b]	39.8 ± 3.9[a,b]	105 ± 2.2	2.52 ± 0.01
LHD_A	1993.3 ± 0.6[c]	46.5 ± 5.1[c]	106.7 ± 5.3	2.61 ± 0.12
LD	2704.1 ± 1.7[d]	65.9 ± 5.5[d]	117.8 ± 7.1	2.80 ± 0.15
LHD	2384.2 ± 4.0	61.7 ± 4.9	143.47 ± 19	3.52 ± 0.49

[a] p = < 0.0001 LD_A vs LHD_A.
[b] p = < 0.0001 LD_A vs LD.
[c] p = < 0.0001 LHD_A vs LHD.
[d] p = < 0.0001 LD vs LHD.

pharmacological outcomes in therapeutic applications [16,41].

3.5. Assessment of in vitro permeation of DMF

Fig. 5a shows the concentrations of DMF detected in the acceptor medium during the in vitro permeation study of LHD and DMF suspensions through synthetic hydrophobic or hydrophilic membranes chosen to simulate the different structure of the nasal mucosa [22]. The corresponding concentrations of MMF are reported in Fig. 5b. When hydrophilic membranes were used, the DMF permeation from LHD was rapid reaching 516.5 µg/mL (corresponding to about 22 % of DMF content) within 15 min and a final value of 623.6 µg/mL (26 %) at 180 min. In contrast, using the hydrophobic membranes, the initial concentration of DMF from LHD was 249.6 µg/mL (11 %), increasing to 502.1 µg/mL at 180 min (about 21 %). DMF from the suspension permeated more rapidly through hydrophilic membranes than through hydrophobic ones in the first 30 min (p < 0.001) (Fig. 5a). As also observed in the in vitro release studies, DMF underwent degradation in acceptor medium, as can be seen from the higher concentration of MMF in the acceptor medium (Fig. 5b): the concentration of MMF was 350.4 µg/mL at 30 min and 413 µg/mL at 240 min when DMF suspension was tested on hydrophilic membrane. MMF was also detected in the acceptor media during the test of LHD (from 18.0 µg/mL at 15 min to 72 µg/mL at 180 min using hydrophilic membranes and from 70 µg/mL at 15 min to

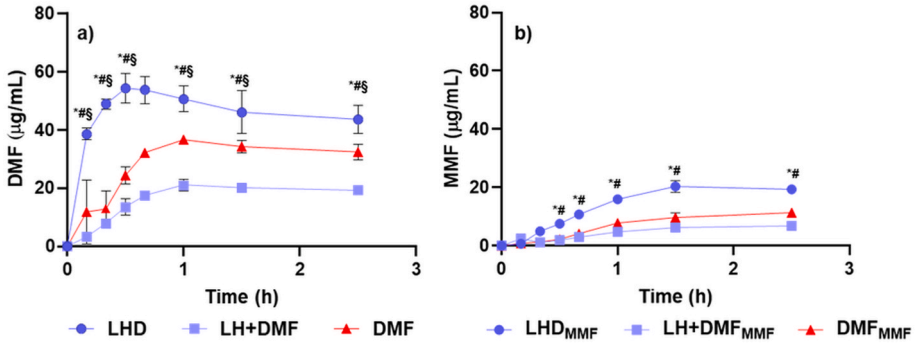

Fig. 4. a) DMF release kinetics from LHD, LH + DMF and DMF suspension for 2.5 h *p < 0.001 LHD vs LH + DMF; #p < 0.001 LHD vs DMF; §p < 0.001 LH + DMF vs DMF; **b)** MMF concentrations in the medium during release test of LHD (LHD_{MMF}), LH + DMF (LH + DMF_{MMF}) and DMF suspension (DMF_{MMF}) for 2.5 h *p < 0.001 LHD_{MMF} vs LH-DMF_{MMF}; #p < 0.001 LHD_{MMF} vs MMF; §p < 0.001 LH + DMF_{MMF} vs MMF. The results are reported as mean ± SD (n = 3).

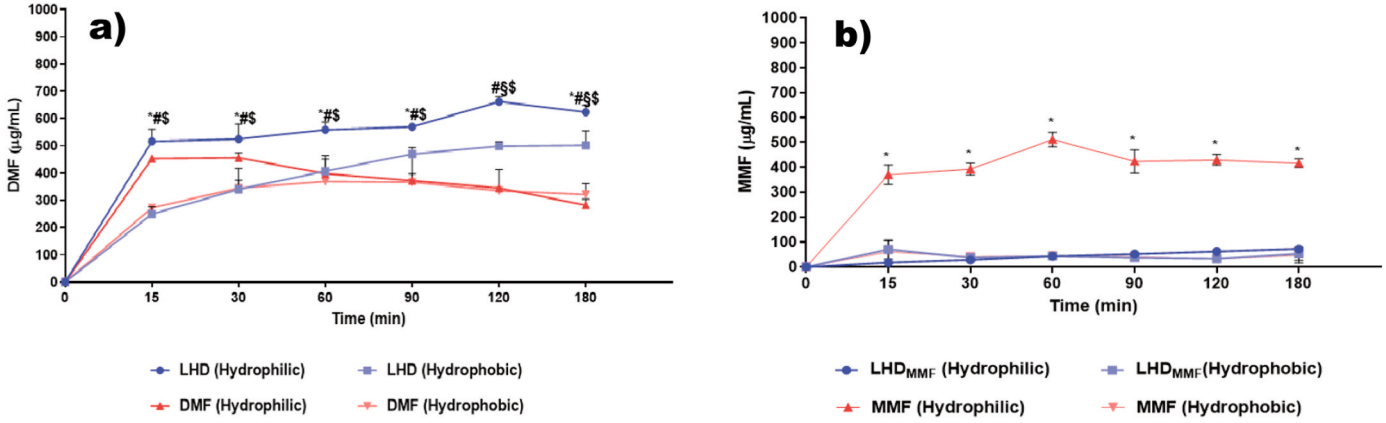

Fig. 5. a) In vitro permeation of DMF aqueous suspension and LHD through hydrophilic and hydrophobic membranes over 180 min (n = 3).; *p < 0.05 LHD hydrophilic vs LHD hydrophobic; #p < 0.001 LHD hydrophilic vs DMF hydrophilic; §p < 0.001 LHD hydrophobic vs DMF hydrophobic; $p < 0.001 DMF hydrophilic vs DMF hydrophobic; **b**) MMF concentrations in acceptor media during in vitro permeation of DMF aqueous suspension and LHD through hydrophilic and hydrophobic membranes over 180 min (n = 3).; *p < 0.05 LHD hydrophilic vs LHD hydrophobic and §p < 0.001 MMF hydrophilic vs MMF hydrophobic.

53 μg/mL at 180 min using hydrophobic membranes). These findings suggest that LHD exhibits substantial in vivo affinity for the hydrophilic components of the nasal mucosa, particularly the mucus layer covering the epithelial surface [22]. This interaction promotes enhanced retention and absorption within the nasal cavity, thereby improving drug delivery. Furthermore, the formulation's ability to permeate the lipophilic membrane of the nasal epithelium is also crucial, as it facilitates the absorption of the active compound into epithelial cells and subsequent entry into systemic circulation [42]. This dual affinity for hydrophilic and lipophilic environments underscores the potential of LHD for effective intranasal delivery of DMF and MMF.

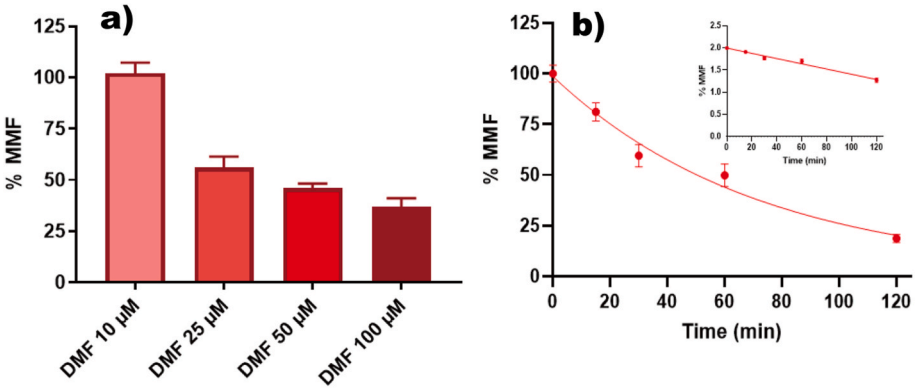

Fig. 6. a) MMF/DMF molar percentage ratios (%MMF) obtained by the DMF hydrolysis in rat whole blood placed in ice bath. DMF stock solutions were added to rat whole blood to obtain final concentrations ranging from 10 to 100 μM and incubated just the time necessary to vortex each sample. The data are reported as the mean ± S.D. of three independent experiments; **b)** Degradation profile of 30 μM MMF in rat whole blood at 37 °C. The degradation of MMF follows a pseudo-first-order kinetic, confirmed by the linearity of the semi-logarithmic plot reported in the inset ($n = 5$, $r = 0.986$, $p < 0.0001$), with a calculated half-life value of 50.97 ± 3.03 min. All data are reported as the mean ± S.E.M. of three independent experiments.

3.6. Stability of DMF and MMF in rat whole blood

DMF was completely degraded within a few seconds after its addition to the rat whole blood, even when the biological sample had been pre-cooled in an ice bath. This result indicates that DMF displays an extremely high tendency to undergo hydrolysis in rat whole blood. Consequently, after the extraction procedures (section 2.9.1), the HPLC analysis revealed a complete absence of DMF and confirmed its hydrolysis to MMF.

The MMF/DMF molar percentage ratio detected in the samples extracted from rat blood decreased as the amount of DMF spiked into the blood increased, as reported in Fig. 6a. In particular, DMF concentrations in rat whole blood ranging from 10 μM to 100 μM resulted in MMF/DMF molar percentage ratios ranging from 100 ± 5 % to 37 ± 4 %. These data suggest that, when present at relatively high concentrations, DMF is not only hydrolysed to MMF but also degraded through other metabolic pathways.

The results reported in Fig. 6a are in good agreement with literature data indicating the high chemical reactivity of the ester groups in DMF, which hydrolyse either spontaneously or by esterases, to form MMF. Moreover, fumaric acid, citric acid and glutathione-adducts are also recognised as products of DMF metabolism in peripheral blood [43,44]. It is worth noting that the DMF half-life in human whole blood at 37 °C is approximatively 6 min [33], indicating that the DMF degradation rate is slower in human than in rat whole blood. This could be due to the fact that the esterase activities are reported to be faster in rodents than in humans [45–48]. Despite these differences, it is relevant to note that after oral administration, either in rats or in humans, DMF is readily hydrolysed to MMF and, consequently, no measurable plasma concentrations of DMF are present, while significant MMF concentrations are detected [49–51]. These data indicate that DMF may be totally metabolized, identifying MMF as the main active metabolite responsible for the in vivo therapeutic effects following the oral administration of DMF [43,50].

Based on the results reported in Fig. 6a, the in vitro stability of MMF in rat whole blood was also assessed by incubating MMF (30 μM) in rat whole blood (37 °C). As reported in Fig. 6b, under these experimental conditions, MMF was degraded over time following a pseudo-first order kinetic, confirmed by the linearity of the semi-logarithmic plot reported in the inset (n = 5, r = 0.986, P < 0.0001), with a half-life value ($t_{1/2}$) = 50.97 ± 3.03 min.

The MMF $t_{1/2}$ in rat whole blood indicates that more than 4 h are required to completely degraded the compound. Therefore, in rat whole blood, the stability of MMF at 37 °C was significantly higher than that of DMF at 0 °C. This result is in agreement with literature data reporting that DMF is more susceptible than MMF to hydrolysis and the formation of glutathione adducts [43,52].

3.7. Intravenous administration of DMF and MMF

In vivo studies were performed to evaluate the pharmacokinetics of MMF following the intravenous administration of the compound or DMF. For this purpose, equivalent molar amounts of MMF and DMF (2.8 μmoles; *i.e.* 0.36 mg and 0.40 mg, respectively, corresponding to a 1.8 mg/kg MMF dose and 2 mg/kg DMF dose) were intravenously infused into the rat femoral vein. Fig. 7 shows the rat plasma MMF concentration-time curves following the intravenous infusion of MMF (Fig. 7a) or DMF (Fig. 7b). In particular, at the end of MMF infusion, its concentration in the bloodstream was 52.1 ± 3.3 μg/mL and decreased over time according to a pseudo first order kinetic confirmed by the linearity of the plot (n = 8, r = 0.997, P < 0.0001) shown in the inset of Fig. 7a. The in vivo $t_{1/2}$ of MMF in the rat bloodstream was calculated as 16.20 ± 0.05 min, a value corresponding to about one-third of the $t_{1/2}$ value obtained in vitro in rat whole blood (50.97 ± 3.03 min, Fig. 6b). Therefore, the degradation by rat blood enzymes plays a significant role in the in vivo elimination processes of MMF. It is interesting to note that the direct administration of a DMF (20 mg/kg in solution) in the rat small intestine led to detect a plasma MMF concentration of about 55 ⌈g/mL [51]. As reported in Fig. 7a, MMF concentration close to 55 μg/mL was obtained in the present study after the intravenous infusion of a molar amount of MMF equivalent to 2 mg/kg of DMF. Overall, these data suggest that only a relatively small portion (not higher than 10 %)

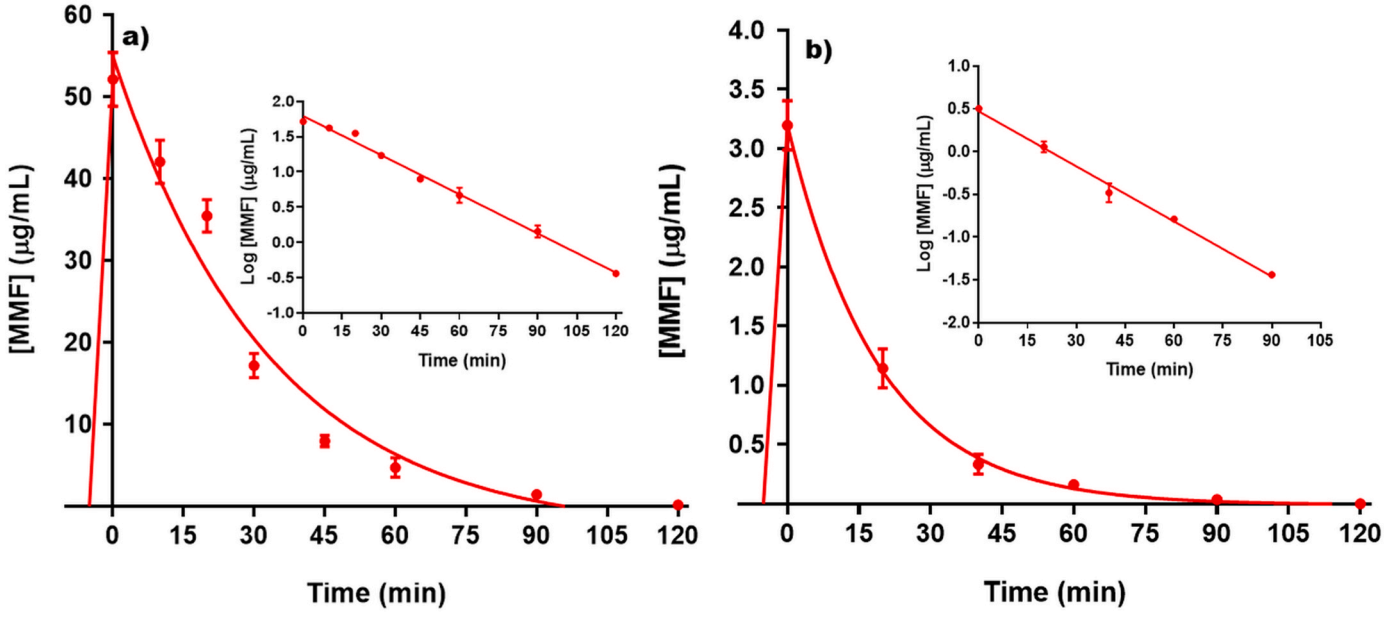

Fig. 7. a) MMF elimination profile after 0.36 mg (1.8 mg/kg) intravenous infusion to rats. The linearity of the semilogarithmic plot reported in the inset (n = 8, r = 0.997, P < 0.0001) confirms the apparent first order kinetic of the MMF elimination from the rat bloodstream. The MMF half-life was calculated to be 16.20 ± 0.05 min. **b)** MMF elimination profile after the intravenous infusion of 0.40 mg (2.0 mg/kg) of DMF. The linearity of the semilogarithmic plot reported in the inset (n = 5, r = 0.997, P < 0.001) confirms the apparent first order kinetic of the MMF elimination from the rat bloodstream. The MMF half-life was calculated to be 13.99 ± 0.05 min. Both the MMF and DMF doses administered correspond to 2.8 ⌈moles of compound. All data are reported as the mean ± S.E.M. of four independent experiments.

of DMF administered in the rat small intestine may reach the bloodstream in the form of its MMF metabolite.

As expected, after the intravenous administration of 2 mg/kg DMF to rats, no measurable plasma concentrations of DMF were detected in plasma already at the first sampling time point (10 min post-dose). This result appears in good agreement with the complete degradation of this compound in rat blood at 4 °C within few seconds (section 3.6). On the other hand, the intravenous administration of DMF (2 mg/kg) allowed to detect its metabolite MMF (Fig. 7b). The amounts of MMF obtained in vivo from DMF were relatively low, in comparison to those obtained by the MMF intravenous administration. Indeed, at the end of the DMF infusion, the MMF concentration in the rat bloodstream was 3.2 ± 0.2 μg/mL; this concentration decreased over time according to a pseudo-first-order kinetic confirmed by the linearity of the plot ($n = 5$, $r = 0.997$, $P < 0.001$) reported in the inset of Fig. 7b. The in vivo half-life ($t_{1/2}$) of MMF was calculated as 13.99 ± 0.05 min, a value very similar to that obtained by the direct intravenous administration of MMF. The AUC values calculated from the plasma MMF concentration-time curves (Fig. 7a and b) were 1653 ± 40 μg·min·mL^{-1} (intravenous administration of 2.8 μmoles of MMF) and 74.7 ± 3.4 μg·min·mL^{-1} (intravenous administration of 2.8 μmoles of DMF). These values indicate that despite the instantaneous degradation of DMF after its intravenous administration, only a small fraction (4.52 % of the total amount administered in the bloodstream) of its hydrolysis product MMF is detected in vivo. Similar results were observed following the oral administration of DMF to humans. Indeed, it was recently reported that after the oral administration of a 240 mg dose of DMF (about 3 mg/kg), only a 5.5 % fraction of MMF was detected in the bloodstream [44]; under the same experimental conditions, the MMF profile showed C_{max} values of approximately 1 μg/mL [50].

In the present study, the concentrations of MMF in rat CSF following the intravenous administration of MMF and DMF (2.8 μmoles; *i.e.,* 0.36 mg and 0.40 mg, respectively, corresponding to a 1.8 mg/kg MMF dose and 2 mg/kg DMF dose), were also measured. As shown in Fig. 8, 10 min after the end of MMF infusion, the compound concentration in CSF was 1.75 ± 0.27 μg/mL and then it decreased to zero within 60 min. This result is in agreement with literature data indicating that a DMF oral dose of 100 mg/kg administered to rats allows to detect MMF in their brain [53]. On the other hand, MMF was undetectable after the intravenous administration of 2 mg/kg DMF, consistent with the low amounts of MMF found in the bloodstream under these experimental conditions.

It is worth noting that the potential ability of MMF to induce direct CNS therapeutic effects against MS remains an open question. Based on the obtained data, and considering that the oral doses of MMF or DMF in humans (about 200 mg; i.e., approximately 3 mg/kg) result in MMF C_{max} values of about 1 μg/mL in the bloodstream [50], it seems unlikely that such doses are sufficient to achieve significant MMF brain targeting.

To the best of our knowledge, this is the first study investigating the in vitro stability of MMF in whole blood, as well as its in vivo pharmacokinetics following the intravenous administration of DMF.

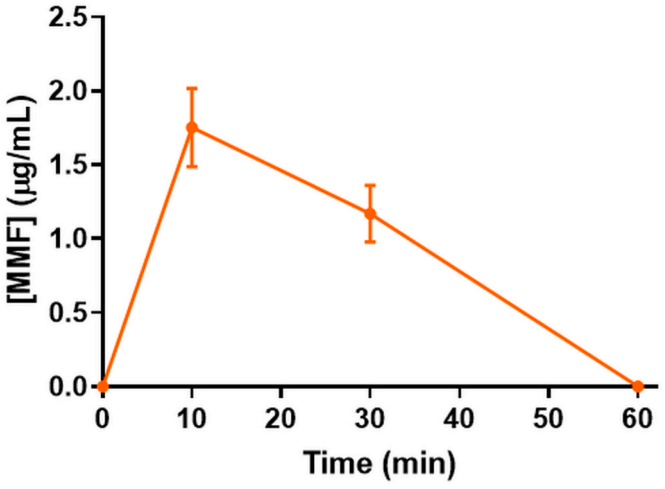

Fig. 8. MMF profile in the CSF of rats after the intravenous administration of 0.36 mg (1.8 mg/kg). The data are reported as the mean ± S.E.M. of four independent experiments.

3.8. Nasal administration of DMF encapsulated in LHD samples

Based on the above results, an LHD nasal formulation was prepared to evaluate its potential ability to target DMF in the CNS.

After the nasal administration of 1 mg/kg of DMF (0.20 mg; LHD) to rats, neither the drug nor its active metabolite MMF was detected in the bloodstream over a period of 3 h. On the other hand, significant amounts of DMF were quantified in the rat CSF, as shown in Fig. 9. In particular, a C_{max} value of 14.4 ± 0.1 μg/mL was detected 30 min (t_{max}) after the end of DMF intravenous administration, after which its concentration decreased to zero within 2 h. Moreover, relatively small amounts of MMF were also detected in the CSF of rats, with concentration values of about 0.15 μg/mL between 20 and 40 min after the administration and decreasing to zero within 90 min from the end of nasal administration. These results indicate that the nasal administration of the LHD formulation allows the DMF brain targeting via a nose-to-brain pathway. The absence of both MMF and DMF in the bloodstream following the LHD nasal administration suggests a selective brain targeting of DMF, with respect to the peripheral compartment of the body. The small amounts of MMF detected in the CSF of rats can be attributed to DMF hydrolysis in the LHD formulation. After the LHD nasal administration, the MMF derived by DMF hydrolysis also appears to be able to reach the CNS.

As a point of comparison, the nasal administration to rats of free DMF as water suspension did not result in the detection of any amounts of the drug or MMF in either the bloodstream or the CSF, indicating the suitability of the LHD nasal formulation for achieving DMF brain targeting. The time required by DMF to reach its C_{max} values in the CSF of rats after the LHD nasal administration suggests that this formulation induces a direct permeation of the drug in CSF across the olfactory mucosa [54–56]. Considering the different pathways proposed to explain the nose-to-brain transport of drugs [36], it can be hypothesized that both extracellular and intracellular pathways are involved in the direct transport of DMF from the nasal mucosa to the CNS. The extracellular pathway is supported by correlating in vivo results with in vitro release and permeation studies. Release studies of DMF from the LHD (Fig. 4) indicate that approximately 30 % of the drug is released within 30 min. This information suggests that the nasal administration of the LHD formulation may allow the free form of DMF to be present in the CSF, which could potentially induce therapeutic effects. The movement of LHD nanoparticles in the CSF of rats seems unlikely, considering that polymeric nanoparticles of about 200 nm in size can cross extracellularly the nasal mucosa only in the presence of absorption promoters, such as chitosan, which are capable of transiently opening the mucosal tight junctions [57,58]. No component of the LHD formulation appears to have this promoting effect; conversely, it has been demonstrated that P does not irritate the mucosal membranes [39], and HA contributes to stabilizing the integrity of the nasal epithelium [59,60]. On the other hand, the intracellular pathway can be directly supported by previous results. In particular, in vitro cell studies on similar hyaluronic acid-coated hybrid nanoparticles demonstrated rapid cellular uptake (from 15 min to 1 h) in both epithelial (RPMI 2650) and neuronal (SK-N-BE2) cell lines [16]. Considering this phenomenon, it appears therefore plausible that the intracellular pathway may contribute to the amount of DMF reaching the CSF, after LHD nasal administration.

Very interestingly, the data reported in Fig. 9 indicate that DMF exhibits great stability at the central level, compared to the bloodstream. Indeed, after a single nasal dose, it takes 2 h for DMF to be completely

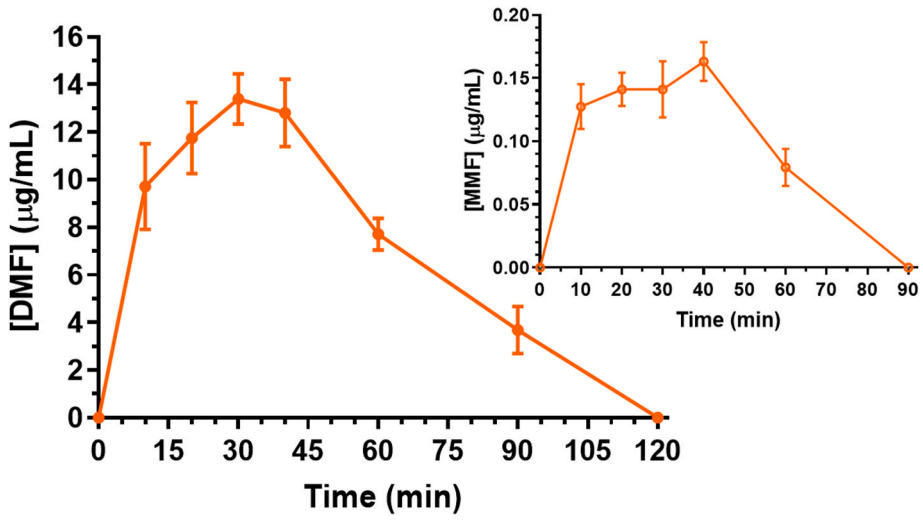

Fig. 9. DMF profile in the CSF of rats after the nasal administration of 0.20 mg (1 mg/kg) encapsulated in the LHD sample. The inset reports the MMF profile obtained by the same nasal administration of DMF. All data are reported as the mean ± S.E.M. of four independent experiments.

eliminated from the CSF of rats, whereas in the bloodstream, it is eliminated almost instantly.

The DMF amounts detected in the rat CSF after nasal administration appear relatively high (the C_{max} value is about 15 μg/mL) suggesting that low volumes of the LHD might be sufficient to achieve therapeutic effects at the central level. In this context, it is worth noting that after the oral administration of DMF therapeutic dosages (about 3 mg/kg), the MMF C_{max} value in the bloodstream was about 1 μg/mL [50].

The above results are particularly relevant as in vitro studies have indicated that DMF is a more potent immune modulator than MMF, capable of reducing the production of pro-inflammatory cytokines [61]; DMF is known to act as a cell protector against oxidative stress by increasing the expression of various antioxidant proteins [62]. Unlike MMF, which does not readily diffuse across plasma membranes due to its negative charge (requiring membrane receptors to produce intracellular effects), DMF readily crosses the cellular membranes and reacts with many intracellular targets [61]. These aspects suggest that LHD, by allowing the brain targeting of DMF and bypassing the bloodstream, may offer new therapeutic perspectives for the use of this drug in MS management.

4. Conclusion

For the delivery and stabilisation of DMF, the simultaneous presence of both lipid and polymeric components, leading to the formation of hybrid nanoparticles, is crucial. The incorporation of hyaluronic acid into lipid-polymer hybrid nanoparticles containing DMF (LHD) significantly improved their physicochemical properties, including particle size, mucoadhesion and viscosity, all of which are essential for effective intranasal drug delivery systems. LHD controlled the release and permeation of DMF in vitro, protecting it from degradation; a small amount of MMF was also present. DMF underwent rapid degradation in both the simulated biological fluid and rat whole blood. Following intranasal administration to rats, LHD enabled direct and selective nose-to-brain transport of DMF in therapeutic dosages, without systemic exposure. These findings provide a deeper understanding of the pharmacokinetics of DMF and open new perspectives for its administration in the treatment of multiple sclerosis, with the potential to address clinical challenges. It can be considered that the clinical benefits of oral DMF are generally attributed to its metabolite MMF; however, in vitro studies suggest that DMF itself exerts stronger immunomodulatory and neuroprotective effects than MMF. Innovative pharmaceutical formulations designed to enhance DMF delivery directly to the brain may therefore open new avenues to improve therapeutic efficacy in MS. Nevertheless, the exact mechanisms of action of both DMF and MMF, particularly within the CNS, remain incompletely understood. Achieving selective CNS delivery could help disentangle their respective neuroinflammatory and neuroprotective effects, potentially leading to the identification of central targets involved in MS pathogenesis and progression, as well as to the development of novel mechanistic hypotheses and therapeutic strategies.

CRediT authorship contribution statement

Carla Serri: Writing – original draft, Visualization, Investigation, Formal analysis, Conceptualization. **Massimo Cossu:** Investigation, Formal analysis, Data curation. **Vincenzo Guarino:** Writing – review & editing, Writing – original draft, Investigation, Formal analysis, Data curation. **Iriczalli Cruz-Maya:** Investigation, Formal analysis, Data curation. **Giada Botti:** Investigation, Formal analysis, Data curation. **Luca Ferraro:** Writing – review & editing, Resources, Investigation, Formal analysis, Data curation. **Paolo Giunchedi:** Validation, Supervision, Resources, Conceptualization. **Giovanna Rassu:** Writing – review & editing, Visualization, Supervision, Project administration, Conceptualization. **Elisabetta Gavini:** Writing – review & editing, Validation, Supervision, Funding acquisition, Conceptualization. **Alessandro Dalpiaz:** Writing – review & editing, Writing – original draft, Visualization, Validation, Resources, Data curation.

Funding

This work was supported by the Foundation of Sardinia (Bando Fondazione di Sardegna 2018–2020 e 2021 – Progetti di ricerca di base dipartimentali"; Grant numbers: J89J21015120005).

Declaration of competing interest

The authors declare that they have no known competing financial interests or personal relationships that could have appeared to influence the work reported in this paper.

Acknowledgement

Authors would like to thank Lipoid GmbH for kindly providing the Lipoid S100® samples. Special thanks to Ms Maria Rosaria Marcedula for the technical support in thermal characterization of materials, Ms.

Maria Cristina del Barone for the technical support in TEM analyses and Dr Mattia Danilo Langellotto for helping in the creation of the graphical abstract using the software BioRender (Langellotto, M. (2025) https://BioRender.com/7gpw458)

Appendix A. Supplementary data

Supplementary data to this article can be found online at https://doi.org/10.1016/j.jddst.2025.107617.

Data availability

Data will be made available on request.

References

[1] M. Haki, H.A. AL-Biati, Z.S. Al-Tameemi, I.S. Ali, H.A. Al-hussaniy, Review of multiple sclerosis: epidemiology, etiology, pathophysiology, and treatment, Medicine (Baltim.) 103 (2024) e37297, https://doi.org/10.1097/MD.0000000000037297.

[2] M. Podbielska, N. Banik, E. Kurowska, E. Hogan, Myelin recovery in multiple sclerosis: the challenge of remyelination, Brain Sci. 3 (2013) 1282–1324, https://doi.org/10.3390/brainsci3031282.

[3] M.P. McGinley, C.H. Goldschmidt, A.D. Rae-Grant, Diagnosis and treatment of multiple sclerosis: a review, JAMA 325 (2021) 765, https://doi.org/10.1001/jama.2020.26858.

[4] L. Higuera, C.S. Carlin, S. Anderson, Adherence to disease-modifying therapies for multiple sclerosis, J. Manag. Care Spec. Pharm. 22 (2016) 1394–1401, https://doi.org/10.18553/jmcp.2016.22.12.1394.

[5] R. Bomprezzi, Dimethyl fumarate in the treatment of relapsing–remitting multiple sclerosis: an overview, Ther. Adv. Neurol. Disord. 8 (2015) 20–30, https://doi.org/10.1177/1756285614564152.

[6] A.D. Kaye, J. Lacey, V. Le, A. Fazal, N.A. Boggio, D.H. Askins, L. Anderson, C. L. Robinson, A. Paladini, C.N. Mosieri, A.M. Kaye, S. Ahmadzadeh, S. Shekoohi, G. Varrassi, The evolving role of monomethyl fumarate treatment as pharmacotherapy for relapsing-remitting multiple sclerosis, Cureus (2024), https://doi.org/10.7759/cureus.57714.

[7] A. Ghods, R. Glick, D. Braun, D. Feinstein, Beneficial actions of the anti-inflammatory dimethyl fumarate in glioblastomas, Surg. Neurol. Int. 4 (2013) 160, https://doi.org/10.4103/2152-7806.123656.

[8] G. Bresciani, F. Manai, S. Davinelli, P. Tucci, L. Saso, M. Amadio, Novel potential pharmacological applications of dimethyl fumarate—an overview and update, Front. Pharmacol. 14 (2023) 1264842, https://doi.org/10.3389/fphar.2023.1264842.

[9] S.A. Scuderi, A. Ardizzone, I. Paterniti, E. Esposito, M. Campolo, Antioxidant and anti-inflammatory effect of Nrf2 inducer Dimethyl fumarate in neurodegenerative diseases, Antioxidants 9 (2020) 630, https://doi.org/10.3390/antiox9070630.

[10] R.A. Linker, R. Gold, Dimethyl fumarate for treatment of multiple sclerosis: mechanism of action, effectiveness, and side effects, Curr. Neurol. Neurosci. Rep. 13 (2013) 394, https://doi.org/10.1007/s11910-013-0394-8.

[11] R. Gold, D.L. Arnold, A. Bar-Or, R.J. Fox, L. Kappos, O. Mokliatchouk, X. Jiang, J. Lyons, S. Kapadia, C. Miller, Long-term safety and efficacy of dimethyl fumarate for up to 13 years in patients with relapsing-remitting multiple sclerosis: final ENDORSE study results, Mult. Scler. J. 28 (2022) 801–816, https://doi.org/10.1177/13524585211037909.

[12] E.S. Cama, L. Catenacci, S. Perteghella, M. Sorrenti, M.R. Caira, G. Rassu, E. Gavini, P. Giunchedi, M.C. Bonferoni, Design and development of a chitosan-based nasal powder of dimethyl fumarate-cyclodextrin binary systems aimed at nose-to-brain administration. A stability study, Int. J. Pharm. 659 (2024) 124216, https://doi.org/10.1016/j.ijpharm.2024.124216.

[13] N. Nieto González, G. Rassu, M. Cossu, L. Catenacci, M.L. Sorrenti, E.S. Cama, C. Serri, P. Giunchedi, E. Gavini, A thermosensitive chitosan hydrogel: an attempt for the nasal delivery of dimethyl fumarate, Int. J. Biol. Macromol. 278 (2024) 134908, https://doi.org/10.1016/j.ijbiomac.2024.134908.

[14] S. Ojha, B. Kumar, H. Chadha, Neuroprotective potential of Dimethyl fumarate-loaded polymeric nanoparticles against multiple sclerosis, Indian J. Pharmaceut. Sci. 81 (2019), https://doi.org/10.36468/pharmaceutical-sciences.535.

[15] S. Ojha, B. Kumar, Preparation and statistical modeling of solid lipid nanoparticles of Dimethyl fumarate for better management of multiple sclerosis, Adv. Pharmaceut. Bull. 8 (2018) 225–233, https://doi.org/10.15171/apb.2018.027.

[16] C. Serri, M. Piccioni, V. Guarino, P. Santonicola, I. Cruz-Maya, S. Crispi, M.P. Di Cagno, L. Ferraro, A. Dalpiaz, G. Botti, P. Giunchedi, G. Rassu, E. Gavini, Hyaluronic acid-based hybrid nanoparticles as promising carriers for the intranasal administration of Dimethyl Fumarate, Int. J. Nanomed. 20 (2025) 71–89, https://doi.org/10.2147/IJN.S481917.

[17] V.P. Chavda, G. Jogi, N. Shah, M.N. Athalye, N. Bamaniya, L. K Vora, A. Cláudia Paiva-Santos, Advanced particulate carrier-mediated technologies for nasal drug delivery, J. Drug Deliv. Sci. Technol. 74 (2022) 103569, https://doi.org/10.1016/j.jddst.2022.103569.

[18] S.-H. Jeong, J.-H. Jang, Y.-B. Lee, Drug delivery to the brain via the nasal route of administration: exploration of key targets and major consideration factors, J. Pharm. Investig. 53 (2023) 119–152, https://doi.org/10.1007/s40005-022-00589-5.

[19] C. Serri, V. Quagliariello, I. Cruz-Maya, V. Guarino, N. Maurea, P. Giunchedi, G. Rassu, E. Gavini, Hyaluronic acid-based nanoparticles loaded with rutin as vasculo-protective tools against anthracycline-induced endothelial damages, Pharmaceutics 16 (2024) 985, https://doi.org/10.3390/pharmaceutics16080985.

[20] A.A. Habib, S.F. Hammad, M.M. Amer, A.H. Kamal, Stability indicating RP-HPLC method for determination of dimethyl fumarate in presence of its main degradation products: application to degradation kinetics, J. Separ. Sci. 44 (2021) 726–734, https://doi.org/10.1002/jssc.202001007.

[21] N. Nieto González, G. Cerri, J. Molpeceres, M. Cossu, G. Rassu, P. Giunchedi, E. Gavini, Surfactant-free chitosan/Cellulose acetate phthalate nanoparticles: an attempt to solve the needs of Captopril administration in paediatrics, Pharmaceuticals 15 (2022) 662, https://doi.org/10.3390/ph15060662.

[22] G. Rassu, E. Soddu, M. Cossu, A. Brundu, G. Cerri, N. Marchetti, L. Ferraro, R. F. Regan, P. Giunchedi, E. Gavini, A. Dalpiaz, Solid microparticles based on chitosan or methyl-β-cyclodextrin: a first formulative approach to increase the nose-to-brain transport of deferoxamine mesylate, J. Contr. Release 201 (2015) 68–77, https://doi.org/10.1016/j.jconrel.2015.01.025.

[23] M.P. Van Den Berg, S.G. Romeijn, J.C. Verhoef, F.W.H.M. Merkus, Serial cerebrospinal fluid sampling in a rat model to study drug uptake from the nasal cavity, J. Neurosci. Methods 116 (2002) 99–107, https://doi.org/10.1016/S0165-0270(02)00033-X.

[24] A. Dalpiaz, L. Ferraro, D. Perrone, E. Leo, V. Iannuccelli, B. Pavan, G. Paganetto, S. Beggiato, S. Scalia, Brain uptake of a zidovudine prodrug after nasal Administration of solid lipid microparticles, Mol. Pharm. 11 (2014) 1550–1561, https://doi.org/10.1021/mp400735c.

[25] A. Madu, C. Cioffe, U. Mian, M. Burroughs, E. Tuomanen, M. Mayers, E. Schwartz, M. Miller, Pharmacokinetics of fluconazole in cerebrospinal fluid and serum of rabbits: validation of an animal model used to measure drug concentrations in cerebrospinal fluid, Antimicrob. Agents Chemother. 38 (1994) 2111–2115, https://doi.org/10.1128/AAC.38.9.2111.

[26] K. Felgenhauer, Protein size and cerebrospinal fluid composition, Klin. Wochenschr. 52 (1974) 1158–1164, https://doi.org/10.1007/BF01466734.

[27] P. Snetkov, K. Zakharova, S. Morozkina, R. Olekhnovich, M. Uspenskaya, Hyaluronic acid: the influence of molecular weight on structural, physical, physico-chemical, and degradable properties of biopolymer, Polymers 12 (2020) 1800, https://doi.org/10.3390/polym12081800.

[28] L. Wu, J. Zhang, W. Watanabe, Physical and chemical stability of drug nanoparticles, Adv. Drug Deliv. Rev. 63 (2011) 456–469, https://doi.org/10.1016/j.addr.2011.02.001.

[29] A. Kovacevic, S. Savic, G. Vuleta, R.H. Müller, C.M. Keck, Polyhydroxy surfactants for the formulation of lipid nanoparticles (SLN and NLC): effects on size, physical stability and particle matrix structure, Int. J. Pharm. 406 (2011) 163–172, https://doi.org/10.1016/j.ijpharm.2010.12.036.

[30] S. Giarra, C. Serri, L. Russo, S. Zeppetelli, G. De Rosa, A. Borzacchiello, M. Biondi, L. Ambrosio, L. Mayol, Spontaneous arrangement of a tumor targeting hyaluronic acid shell on irinotecan loaded PLGA nanoparticles, Carbohydr. Polym. 140 (2016) 400–407, https://doi.org/10.1016/j.carbpol.2015.12.031.

[31] T.A. Korolenko, T.P. Johnston, N.V. Tamkovich, V.A. Vavilin, N.P. Bgatova, I. D. Ivanov, G.S. Russkikh, E.V. Koldysheva, E.C. Korolenko, V.I. Kapustina, S. I. Makarova, N.V. Goncharova, M.M. Gevorgyan, V.M. Loginova, The effects of pretreatment with atorvastatin, fenofibrate, or both drugs in a mouse model of acute lipemia induced by the general lipase inhibitor poloxamer 407, Biochem. Mosc. Suppl. Ser. B Biomed. Chem. 18 (2024) 214–230, https://doi.org/10.1134/S1990750823600474.

[32] L. Wang, N. Dos Santos Sanches, L. Panahipour, A. Imani, Y. Yao, Y. Zhang, L. Li, R. Gruber, Dimethyl fumarate-loaded gellan gum hydrogels can reduce in vitro chemokine expression in oral cells, Int. J. Mol. Sci. 25 (2024) 9485, https://doi.org/10.3390/ijms25179485.

[33] N.H. Litjens, E. Van Strijen, C. Van Gulpen, H. Mattie, J.T. Van Dissel, H.B. Thio, P. H. Nibbering, In vitro pharmacokinetics of anti-psoriatic fumaric acid esters, BMC Pharmacol. 4 (2004) 22, https://doi.org/10.1186/1471-2210-4-22.

[34] Y. Liu, Y. Liang, J. Yuhong, P. Xin, J.L. Han, Y. Du, X. Yu, R. Zhu, M. Zhang, W. Chen, Y. Ma, Advances in nanotechnology for enhancing the solubility and bioavailability of poorly soluble drugs, Drug Des. Dev. Ther. 18 (2024) 1469–1495, https://doi.org/10.2147/DDDT.S447496.

[35] I.S. Bayer, Recent advances in mucoadhesive interface materials, mucoadhesion characterization, and technologies, Adv. Mater. Interfac. 9 (2022) 2200211, https://doi.org/10.1002/admi.202200211.

[36] M.L. Formica, D.A. Real, M.L. Picchio, E. Catlin, R.F. Donnelly, A.J. Paredes, On a highway to the brain: a review on nose-to-brain drug delivery using nanoparticles, Appl. Mater. Today 29 (2022) 101631, https://doi.org/10.1016/j.apmt.2022.101631.

[37] M. Nasr, Development of an optimized hyaluronic acid-based lipidic nanoemulsion co-encapsulating two polyphenols for nose to brain delivery, Drug Deliv. 23 (2016) 1444–1452, https://doi.org/10.3109/10717544.2015.1092619.

[38] M. King, B.K. Rubin, Pharmacological approaches to discovery and development of new mucolytic agents, Adv. Drug Deliv. Rev. 54 (2002) 1475–1490, https://doi.org/10.1016/S0169-409X(02)00156-4.

[39] E. Giuliano, D. Paolino, M. Fresta, D. Cosco, Mucosal applications of poloxamer 407-Based hydrogels: an overview, Pharmaceutics 10 (2018) 159, https://doi.org/10.3390/pharmaceutics10030159.

[40] S. Mansuri, P. Kesharwani, K. Jain, R.K. Tekade, N.K. Jain, Mucoadhesion: a promising approach in drug delivery system, React. Funct. Polym. 100 (2016) 151–172, https://doi.org/10.1016/j.reactfunctpolym.2016.01.011.

[41] L. Mayol, F. Quaglia, A. Borzacchiello, L. Ambrosio, M. Rotonda, A novel poloxamers/hyaluronic acid in situ forming hydrogel for drug delivery: rheological, mucoadhesive and in vitro release properties, Eur. J. Pharm. Biopharm. 70 (2008) 199–206, https://doi.org/10.1016/j.ejpb.2008.04.025.
[42] M. Ghadiri, P.M. Young, D. Traini, Strategies to Enhance Drug Absorption via Nasal and Pulmonary Routes, Pharmaceutics 11 (2019) 113. https://doi.org/10.3390/pharmaceutics11030113.
[43] U. Mrowietz, P.J. Morrison, I. Suhrkamp, M. Kumanova, B. Clement, The pharmacokinetics of fumaric acid esters reveal their in vivo effects, Trends Pharmacol. Sci. 39 (2018) 1–12, https://doi.org/10.1016/j.tips.2017.11.002.
[44] L. Xu, C.-C. Peng, K. Dawson, S. Stecher, J. Woodworth, C. Prakash, Metabolism, pharmacokinetics and excretion of [^{14} C]dimethyl fumarate in healthy volunteers: an example of xenobiotic biotransformation following endogenous metabolic pathways, Xenobiotica 53 (2023) 163–172, https://doi.org/10.1080/00498254.2023.2217506.
[45] P.D. Jobsis, E.C. Rothstein, R.S. Balaban, Limited utility of acetoxymethyl (AM)-based intracellular delivery systems, *in vivo* : interference by extracellular esterases, J. Microsc. 226 (2007) 74–81, https://doi.org/10.1111/j.1365-2818.2007.01755.x.
[46] A. Dalpiaz, G. Paganetto, B. Pavan, M. Fogagnolo, A. Medici, S. Beggiato, D. Perrone, Zidovudine and ursodeoxycholic acid conjugation: design of a new prodrug potentially able to bypass the active efflux transport systems of the central nervous system, Mol. Pharm. 9 (2012) 957–968, https://doi.org/10.1021/mp200565g.
[47] K.M. Huttunen, Identification of human, rat and mouse hydrolyzing enzymes bioconverting amino acid ester prodrug of ketoprofen, Bioorg. Chem. 81 (2018) 494–503, https://doi.org/10.1016/j.bioorg.2018.09.018.
[48] J. Lian, R. Nelson, R. Lehner, Carboxylesterases in lipid metabolism: from mouse to human, Protein Cell 9 (2018) 178–195, https://doi.org/10.1007/s13238-017-0437-z.
[49] N.H.R. Litjens, J. Burggraaf, E. Van Strijen, C. Van Gulpen, H. Mattie, R. C. Schoemaker, J.T. Van Dissel, H.B. Thio, P.H. Nibbering, Pharmacokinetics of oral fumarates in healthy subjects, Br. J. Clin. Pharmacol. 58 (2004) 429–432, https://doi.org/10.1111/j.1365-2125.2004.02145.x.
[50] T.W. Lategan, L. Wang, T.N. Sprague, F.S. Rousseau, Pharmacokinetics and bioavailability of monomethyl fumarate following a single oral dose of Bafiertam^{TM} (Monomethyl fumarate) or tecfidera® (Dimethyl fumarate), CNS Drugs 35 (2021) 567–574, https://doi.org/10.1007/s40263-021-00799-9.
[51] S. Dibbert, B. Clement, T. Skak-Nielsen, U. Mrowietz, M. Rostami-Yazdi, Detection of fumarate–glutathione adducts in the portal vein blood of rats: evidence for rapid dimethylfumarate metabolism, Arch. Dermatol. Res. 305 (2013) 447–451, https://doi.org/10.1007/s00403-013-1332-y.
[52] S. Schilling, S. Goelz, R. Linker, F. Luehder, R. Gold, Fumaric acid esters are effective in chronic experimental autoimmune encephalomyelitis and suppress macrophage infiltration, Clin. Exp. Immunol. 145 (2006) 101–107, https://doi.org/10.1111/j.1365-2249.2006.03094.x.
[53] B.T. Wipke, R. Hoepner, K. Strassburger-Krogias, A.M. Thomas, D. Gianni, S. Szak, M.S. Brennan, M. Pistor, R. Gold, A. Chan, R.H. Scannevin, Different fumaric acid esters elicit distinct pharmacologic responses, Neurol. Neuroimmunol. Neuroinflammation 8 (2021) e950, https://doi.org/10.1212/NXI.0000000000000950.
[54] L. Illum, Transport of drugs from the nasal cavity to the central nervous system, Eur. J. Pharmaceut. Sci. 11 (2000) 1–18, https://doi.org/10.1016/S0928-0987(00)00087-7.
[55] M. Agrawal, S. Saraf, S. Saraf, S.G. Antimisiaris, M.B. Chougule, S.A. Shoyele, A. Alexander, Nose-to-brain drug delivery: an update on clinical challenges and progress towards approval of anti-alzheimer drugs, J. Contr. Release 281 (2018) 139–177, https://doi.org/10.1016/j.jconrel.2018.05.011.
[56] G. Botti, A. Dalpiaz, B. Pavan, Targeting systems to the brain obtained by merging prodrugs, nanoparticles, and Nasal administration, Pharmaceutics 13 (2021) 1144, https://doi.org/10.3390/pharmaceutics13081144.
[57] I. Schlachet, A. Sosnik, Protoporphyrin IX-modified chitosan-g-oligo(NiPAAm) polymeric micelles: from physical stabilization to permeability characterization in vitro, Biomater. Sci. 5 (2017) 128–140, https://doi.org/10.1039/C6BM00667A.
[58] I. Schlachet, A. Sosnik, Mixed mucoadhesive amphiphilic polymeric nanoparticles cross a model of Nasal septum Epithelium in vitro, ACS Appl. Mater. Interfaces 11 (2019) 21360–21371, https://doi.org/10.1021/acsami.9b04766.
[59] G.D. Albano, A. Bonanno, D. Giacomazza, L. Cavalieri, M. Sammarco, E. Ingrassia, R. Gagliardo, L. Riccobono, M. Moscato, G. Anzalone, A.M. Montalbano, M. Profita, A 3D " *In Vitro* " model to Study hyaluronan effect in nasal epithelial cell line exposed to double-stranded RNA Poly(I:C), Biomol. Ther. 28 (2020) 272–281, https://doi.org/10.4062/biomolther.2019.126.
[60] S. Tuncay Tanriverdi, E.H. Gokce, I. Sušanj, L. Simić, K. Vukelić, Z. Knežević, P. Ilhan, A. Sendemir, O. Ozer, Comprehensive evaluation of xylometazoline hydrochloride formulations: Ex-vivo and in-vitro studies, Eur. J. Pharm. Biopharm. 203 (2024) 114466, https://doi.org/10.1016/j.ejpb.2024.114466.
[61] C. Dello Russo, K.A. Scott, M. Pirmohamed, Dimethyl fumarate induced lymphopenia in multiple sclerosis: a review of the literature, Pharmacol. Ther. 219 (2021) 107710, https://doi.org/10.1016/j.pharmthera.2020.107710.
[62] S.K. Yadav, D. Soin, K. Ito, S. Dhib-Jalbut, Insight into the mechanism of action of dimethyl fumarate in multiple sclerosis, J. Mol. Med. 97 (2019) 463–472, https://doi.org/10.1007/s00109-019-01761-5.